Zhao et al. Environ Syst Res (2016) 5:21
DOI 10.1186/s40068-016-0072-3

Environmental Systems Research

RESEARCH Open Access

Prevention of stack corrosion under wet flue gas desulfurization conditions in a coal-fired power plant: performance analysis and comparative study

Shan Zhao[1], Yi Zhao[2*], Yinghui Han[3], Chunjiang An[1], Jia Wei[4] and Yao Yao[1]

Abstract

Background: This study investigated the prevention of stack corrosion under wet flue gas desulfurization conditions in a coal-fired power plant. The performance analysis and comparative studies of six materials for the prevention of stack corrosion were investigated.

Results: The ion chromatography analysis showed the acid condensation contained fluoride, chloride, nitrate, sulphate, and sulphite. The weight loss method showed titanium alloy and foam glass blocks were heat and acid resistant. The scanning electron microscopy indicated the morphologies were pits, cracks, and flakes for sulfuric acid dew corrosion resistant steel, and X-ray diffraction showed the corrosion products mainly consisted of Fe_2O_3, $FeSO_4$, FeOOH, with some Fe_3O_4 or FeF_3. The comparative study indicated that cyclic wet-dry conditions resulted in more aggressive corrosion to the stack than acid condensation.

Conclusions: Titanium alloy and foam glass blocks had the best performance and could be applied in the stack to prevent corrosion. The effects of cyclic wet-dry conditions should be taken into account to mitigate stack corrosion in coal-fired power plants.

Keywords: Wet flue gas desulfurization, High temperature corrosion, Acid corrosion, Cyclic wet-dry environment, Coal-fired power plant

Background

Wet lime/limestone flue gas desulfurization technology has become one of the leading flue gas desulfurization techniques in many power plants around the world, owing to its advantages of high desulfurization efficiency, wide adaptation and long-run stability etc. (ZareNezhad and Aminian 2010; Gutiérrez Ortiz and Ollero 2008; Zhao et al. 2011a, b). However, it also brings about serious corrosion problems to the inner wall of stacks. In this way, it is indispensable to protect stacks from corrosion after the wet flue gas desulfurization (WFGD) system. Power plant stacks are mainly operated in the following three conditions: (1) the complete withdrawal of WFGD (bypass fully open). If not passing WFGD, the flue gas is above 120 °C. The interior wall is completely dry and the flue gas brings no direct corrosion to the stack; (2) the complete input of WFGD (bypass fully closed). Following WFGD without the installment of gas gas heater (GGH), the flue gas entering stack is at 50 °C and of high humidity. Meanwhile, considerable acid condensation occurs on the stack inner wall and the acid even starts to accumulate or flow, which is a symbol of serious corrosion; (3) the partial withdrawal of WFGD (bypass partially open). In this case, high-temperature dry flue gas without desulfurization would mix with low-temperature wet flue gas with desulfurization at the entrance of stack, and then a more complex corrosion environment would be formed under such cyclic wet-dry conditions. In all, acid

*Correspondence: zhaoyi9515@163.com
[2] School of Environmental Science and Engineering, North China Electric Power University, Baoding 071003, People's Republic of China
Full list of author information is available at the end of the article

condensation problems always exist in stack following WFGD without GGH. Therefore, the alternating operation of the three running conditions would call for materials that are more corrosion resistant.

Many studies on corrosion resistance of substrate have focused on the employment of certain materials, like coatings, linings, and lightweight insulation products (Noubactep 2010). The advantages of good adhesion, high humidity tolerance, and chemical and solvent resistance have been reported for polyurea, and this material has been successfully utilized to promote adhesion and protect the substrate from corrosion (Ni et al. 2002). Data supports that epoxy glass coating is better for the protection of carbon steel since the barrier characteristics of the film against water transport could provide corrosion protection to the underlying metal (González-Guzmán et al. 2010). This material is able to protect metal from corrosion in highly corrosive media because it is expected to greatly hinder the water transport through the polymeric matrix (ZareNezhad and Aminian 2010). Moser et al. (2011) have conducted certain experiments on fiber reinforced plastic, concluding that this material is able to show excellent corrosion resistance in different positions in the plant (prescrubber unit, absorber, and desorber) at a wide range of specific process conditions (temperature, pressure, solvent loading, and gas/solvent stream). Corrosion resistant steel for sulfuric acid dew is a type of low-alloy structural steel, including a small amount of manganese, copper, chromium, antimony, nickel, or tin, to form a protective layer on the metal surface. Jeon et al. (2011) and Nam et al. (2010) confirmed that the interactions of tin with copper and antimony improve the corrosion resistance of low-alloy steel owing to the formation of the continuous tin oxide, copper oxide and antimony oxide layer. The outstanding corrosion resistance of titanium alloy is achieved by the complementary effect of co-implantation with metal ions. Co-implantation is a possible process for attaining excellent corrosion protection of titanium against aggressive environments (Sugizaki et al. 1996). Foam glass blocks are mainly composed of borosilicate. The joining properties involving bonding strength, thermal shock resistance and corrosion resistance were systematically investigated and experimentally demonstrated (Song et al. 2011). It has been reported that borosilicate material is able to undergo surface restoration at elevated temperatures since it has the tendency to form protective layers below and above the surface line (Soo Park et al. 1999).

Currently, the control of stack corrosion is limited to theoretical analysis at high temperature or in acid condensation only. The real operating conditions in stack under WFGD conditions have rarely been simulated before. Furthermore, there is a lack of comparative studies of the stack corrosion in acid condensation and cyclic wet-dry environments. The corrosion behavior of stack in cyclic wet-dry conditions and the corresponding mechanisms have received little attention.

In this study, a performance analysis and comparative study were conducted to investigate the prevention of stack corrosion under WFGD conditions in coal-fired power plants. Comparing the effects of cyclic wet-dry condition and acid condensation on various materials, the corrosion resistance and mechanisms were investigated experimentally; and further the comparative studies were performed to find materials that could be applied in stacks. The objectives were to evaluate the performance of materials in acid condensation and cyclic wet-dry environments, and to mitigate the corrosion in stacks under WFGD conditions in coal-fired power plants.

Methods

Materials

Based on lab experiments and engineering practice, polyurea, epoxy glass coatings, fiber reinforced plastics, corrosion resistant steels, titanium alloy and foam glass blocks are widely used (Ni et al. 2002; González-Guzmán et al. 2010; Moser et al. 2011; Jeon et al. 2011; Nam et al. 2010; Sugizaki et al. 1996; Song et al. 2011; Soo Park et al. 1999). In this study, polyurea and vinyl ester glass flake (VEGF) were classified as the coating materials; titanium alloy, sulfuric acid dew corrosion resistant steel (ND) and fiberglass reinforced plastics (FRP) were selected as the lining materials; foam glass blocks were deemed as the lightweight insulation products. The chemical compositions of the six materials are listed in Table 1. Polyurea is a type of elastomer that is derived from the reaction product of an isocyanate component and a synthetic resin blend component through step-growth polymerization. The molecule has two amine groups ($-NH_2$) joined by a carbonyl functional group ($-C=O$). The main constituent of VEGF is phenolic epoxy vinyl ester resin, which is produced by the esterification of an epoxy resin with an unsaturated monocarboxylic acid. FRP is one composite material of glass fibers combined with 191 unsaturated polyester resins. Titanium alloy is made of Ti mixed with Ni and Mo together, while ND steel is Fe with elements such as Mn, Cu, and Cr, etc. As for foam glass block, it mainly consists of borosilicate glasses. All the following experiments and analysis were performed based on these six selected materials.

Acid condensation analysis

Ion chromatography was used to clarify the constituents in the acid condensation from a power plant stack of Shandong province in China. The anion standard series were performed to further measure the species and content of ions in the samples. The test solutions were

Table 1 Chemical composition of the experimental materials

Materials	Composition
Polyurea	$*\text{-}[\text{NHCONH}]_n\text{-}*$
VEGF	$*\text{-}[\text{C}_6\text{H}_6\text{O}\cdot\text{C}_3\text{H}_5\text{ClO}\cdot\text{CH}_2\text{O}]_n\text{-}*$
FRP in wt%	53.3 of 191-unsaturated polyester resin reinforced with 46.7 of fiberglass
Titanium alloy in wt%	Ti with 0.40 Mo, 0.90 Ni, 0.30 Fe, 0.08 C, 0.03 N, 0.015 H, 0.25 O
ND steel in wt%	Fe with 0.07 C, 0.56 Cr, 0.12 Ni, 0.29 Cu, 0.44 Mn, 0.073 Sb, 0.05 Sn, 0.011 P, 0.20 Si, 0.008 S, 0.014 Ti
Foam glass blocks	Borosilicate glass mixed with foaming agent, etc.

VEGF vinyl ester glass flake, *FRP* fiberglass reinforced plastics, *ND* sulfuric acid dew corrosion resistant steel

prepared by analytical grade chemicals and ultrapure water based on the analytical results.

High temperature and variable temperature test

High temperature tests and variable temperature tests were conducted to investigate the temperature resistance of each material. Five replicates were included in each material group. For the high temperature test, the samples were first placed in the drying oven at 120 °C for 6 h. After observation, they were then placed under 180 °C for another 6 h. In terms of the variable temperature test, the samples were kept inside the drying oven, and the temperature was alternating back and forth from 50 to 180 °C for five times. At each interval, the temperature was maintained at 50 or 180 °C for 6 h.

Accelerated corrosion test

In order to further evaluate the impact of both temperature and acidity on stack materials, two sets of accelerated corrosion experiments were designed. The first group established the temperature at 50 °C and materials were immersed in static acid condensation for 6 days, a total of 144 h. The second group set the high temperature at 120 °C, while low temperature at 50 °C to simulate the cyclic wet-dry environment in power plant stacks. Materials in the second group were immersed in low-temperature acid for 18 h before put in high-temperature environments for 3 h each day. This summed up to a total of 108 h' immersion in acid solution. Ten samples were divided into two groups for each material. Four replicates were soaked in the static low-temperature acid condensation; and the rest one was treated as a blank in the first group. Four replicates underwent the cyclic wet-dry test; and the rest one was similarly treated as a blank for calibration in the second group.

Analytical methods

The anion species and content analysis were performed using Metrohm ion chromatograph (IC 792 plus ASupp4 Anion separation column, Metrohm in Switzerland). The eluent conditions were listed as below (Zivojinovic and Rajakovic 2011; Sedyohutomo et al. 2008): the concentrations of $NaHCO_3$ and Na_2CO_3 solution were 4 and 1.4 mmol/L, respectively; the mass fraction of $CH_3C\text{-}OCH_3$ was 5 %; pH was 9.92; the flow rate was 1 mL/min. The purpose of adding acetone into the eluent was to make sulfite and sulfate peaks well separated. In order to control concentration of analyte below 100 mg/L, the test solution was initially diluted 50 times with eluent before use. The pH value was measured with digital pH meter (pHS-3C, Hangzhou ally dragon instrument, China) and sulfuric acid was used as pH adjustment.

As for the temperature tests, visual method was used to study the surface change of the samples, and the weight loss method was employed to record mass decrease of the samples. As for the accelerated corrosion tests, the corrosion rate of each material was initially identified by weight loss measurement (Jang et al. 2009). According to ASTM G1 standard (Siamphukdee et al. 2013), the corrosion rate (mm/y) was calculated as Eq. (1):

$$\text{Corrosion rate} = \frac{K \times W}{A \times t \times \rho} \quad (1)$$

where K is the constant in (mm h)/(year cm)—87,600, W is the mass loss in grams, A *is* the coupon exposed area in cm^2, t *is* the time of exposure in hours and ρ is the specific mass of the experimental material in g/cm^3, respectively. The specimens were conventionally prepared by grinding with silicon carbide paper and by diamond polishing. Thereafter, they were ultrasonically degreased and rinsed in acetone, and then were dried and weighed before the start of the tests. Samples were weighed using the electronic scale with the resolution of 0.0001 g (AB104-N type, Mettler in Switzerland). After the tests, the specimens with films were dried and weighed again. Afterwards, cold field emission scanning electron microscopy (CFP-SEM, JSM-7500F model, Japan Electronics Corporation) was employed to acquire information of the morphology characteristics of ND steel and scanning electron microscopy (SEM, KYKY2800B, KYKY in China) for the

foam glass blocks. Furthermore, X-ray diffraction (XRD, D8 ADVANCE type, BRUKER-AXS in Germany) was performed to clarify the possible corrosion mechanism of ND steel. All data reported were the average of at least three independent samples and the typical error in the measurement was less than 10 %.

Results and discussion

Characterization of anions in acid condensation

The acid condensation was taken from the stack of # 1 and # 2 units in Laicheng power plant, which is located in Shandong province, China. The two units share a stack and there is no GGH installed in these two units following WFGD system. The anion species and content of the acid condensation were initially determined through ion chromatography. Furthermore, based on the data and parameters achieved, experimental acid condensation would be simulated for the following accelerated corrosion test in this study.

After the filtration treatment on the acid condensation samples, the type and the concentration of the anions were measured respectively and the results are shown in Table 2. From the chromatogram, it could be concluded that the acid condensation mainly contains F^-, Cl^-, NO_3^- and SO_4^{2-}. The dissolution of SO_4^{2-} leads to the formation of sulfuric acid, which is highly corrosive to the stack. When analyzing corrosive anions in conditioned water-steam cycles, F^-, Cl^-, NO_3^-, PO_4^{3-} and SO_4^{2-} have been observed (Zivojinovic and Rajakovic 2011) using $NaHCO_3/Na_2CO_3$ solution as the eluent. F^-, Cl^-, NO_3^- and SO_4^{2-} have also been detected in condensed steam of geothermal power plants (Santoyo et al. 2002). Meanwhile, F^-, CH_3COO^-, Cl^-, NO_3^-, SO_4^{2-}, Br^-, NO_2^- and PO_4^{3-} have been found in power plant water samples (Lu et al. 2002), respectively.

According to the analysis results, the stack acid condensation mainly contained F^-, Cl^-, NO_3^- and SO_4^{2-}. According to the data reported in literature (Zivojinovic and Rajakovic 2011; Sedyohutomo et al. 2008; Hu et al. 2000), a small amount of sulfite SO_3^{2-} was supposed to exist in acid condensation, which might be oxidized to SO_4^{2-} during sampling and storage process without being detected. Therefore, a small amount of SO_3^{2-} was added in the preparation and simulation of acid condensation, with the concentration of 100 mg/L. In all, the composition of the experimental acid condensation and pH were: F^- 39.45 mg/L; Cl^- 114.4 mg/L, NO_3^- 106.75 mg/L, SO_4^{2-} 2934.65 mg/L, SO_3^{2-} 100 mg/L, and pH 1.5, as shown in Table 2.

High temperature test

The test was performed to investigate the resistance of six materials at high temperature, and the results are denoted in the Fig. 1a. It can be observed that the mass loss for VEGF was significantly higher than the other materials under the same condition. After experiments at 120 °C for 6 h and 180 °C for another 6 h, the mass loss of VEGF was as high as 17.11 mg/cm^2, indicating VEGF was especially unstable and was prone to volatilization at high temperature. Long periods of utilization might cause corrosion failure of power plant stacks. Moreover, the mass loss of polyurea and FRP were 1.21 and 1.48 mg/cm^2, respectively, which were relatively low. High temperature had no effect on titanium alloy and ND steel owing to the fast thermal conductivity as metals. Foam glass blocks were also qualified due to its superior thermal diffusivity.

As shown in Fig. 1a, the minor mass loss of polyurea indicated insignificant evaporation under high temperature conditions. Other than discoloration, polyurea coatings did not change significantly, and the junction of its cross-section with the steel substrate did not crack, because of the thermal expansion difference. Spalling or other adhesion issues did not occur. The superior heat resistance properties were also verified by Qiao et al. (2011) in the designed dynamic mechanical analysis. For polyurea, a slight weight decrease was consistent with the appearance change, indicating that polyurea was basically resistant to hot flue gas, and could be applied to high temperature conditions of power plant stack.

After experiments under 120 °C for 6 h, no significant change occurred to the specimen surface, indicating the temperature of 120 °C played little effect on the performance of VEGF. However, a clear volatilization and mass loss occurred to the organic components under 180 °C for 6 h. Cracking and peeling also appeared on the surface of the organic coating. These all demonstrated that even short periods of thermal shock could place a significant effect on the corrosion resistance of VEGF. As for FRP, the organic component volatilized slightly under high temperature. However, the samples became yellow and deformed, which were notable signs of degradation.

Table 2 Anion types and concentrations of the acid condensation

Anion (mg/L)	F^-	Cl^-	NO_3^-	SO_4^{2-}	SO_3^{2-}
Measured concentration in stack	39.45 ± 1.57	114.4 ± 8.18	106.75 ± 10.54	2934.65 ± 194.57	/
Concentration in this study	39.45	114.4	106.75	2934.65	100

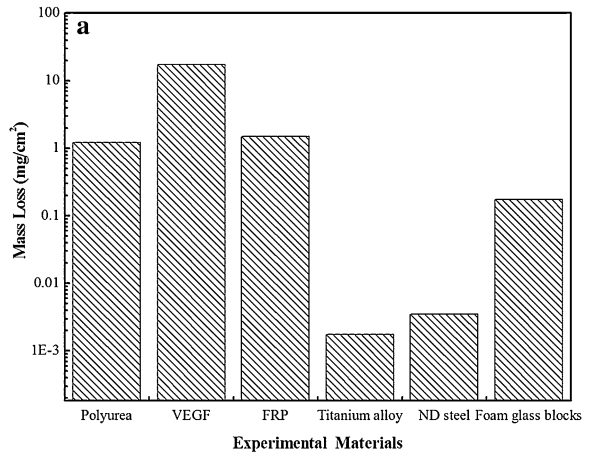

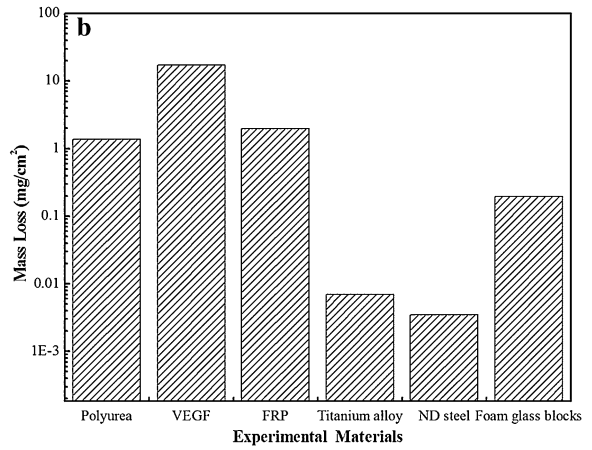

Fig. 1 Mass loss of six experimental materials under various conditions: **a** 120 °C for 6 h and 180 °C for another 6 h; **b** alternating back and forth from 50 to 180 °C for 30 h

Even if the material was under hot environment shortly, this may affect the corrosion resistance of FRP.

VEGF mainly consisted of epoxy vinyl phenolic resin, and the color change probably because the molecular chain of the phenolic groups was prone to degradation under high temperature, manifesting as coking, yellowing, or loss of gloss on its appearance. The deformation of FRP might have occurred because the molecular chains stretch at high temperature but fail to shrink back into the original state when the temperature decreases. Russel (2011) summarized that deformation can be either elastic or viscous. The former often led to cracking and peeling, while the latter produced a pore-free solid. Roberts et al. (2011) concluded that deformation results in dramatic color change at high temperatures, although the films had to be irreversibly elastically deformed to achieve this. It can be concluded that VEGF could withstand the temperature of 120 °C, but was unable to withstand the thermal shock of 180 °C. Thus, VEGF may be damaged by the high temperature flue gas of power plant bypass. The utilization of FRP may cause corrosion failure under the long-running process of power plant stacks.

The weight and appearance of titanium alloy, ND steel and foam glass blocks did not change considerably because of their excellent heat resistance, high thermal conductivity and superior heat dissipation properties. Cai et al. (2010) reported that the tensile ductility of TG6 titanium alloy increases rapidly, and its thermal stability gets a recovery to a great extent once the temperature rises over 150 °C. The heat resistance of a low alloy steel was demonstrated by Ghanem et al. (1996) through measuring the weight of the corrosion product film on the alloy surface over exposure times up to 480 h, and at a temperature range of 75–250 °C. The higher temperature induces better anti-corrosion behavior of borosilicate due to the low viscosity studied by Song et al. (Grujicic et al. 2010). These facts indicated that titanium alloy, ND steel and foam glass blocks all could be applied to the high temperature conditions in power plant chimneys.

Variable temperature test

The test was conducted to study the resistance of six materials to variable temperature. In view of Fig. 1b, it could clearly be seen that VEGF underwent dramatic mass loss after the variable temperature test. Conversely, polyurea, titanium alloy, ND steel and foam glass blocks all behaved well in the same corrosion environment. From another standpoint, FRP was not suitable for the condition because of its significant appearance change. The same conclusion could be attained that as for the six materials, VEGF and FRP were not suitable to be employed under the high temperature and variable temperature environments in power plant stacks.

As shown in Fig. 1b, polyurea samples with a mass loss of 1.36 mg/cm^2 volatilized slightly under variable temperature. After five times of alternating temperature change, the overall appearance of polyurea did not alter significantly. Grujicic et al. (2010) revealed that an increase in the test temperature caused an increase in the strain-rate associated with the maximum glass-transition based energy absorption/dissipation. Polyurea tended to display high-ductility behavior of a stereotypical elastomer in its rubbery-state. As for polyurea, minor changes of mass and appearance demonstrated that polyurea embraced good temperature resistance and was suitable for the variable temperature conditions in power plant stacks.

The mass loss for VEGF is 17.01 mg/cm^2, which indicating that the organic ingredients volatilized remarkably under variable temperature conditions. The color of VEGF became remarkably yellow and dull from the appearance. While the mass loss of FRP is 1.96 mg/cm^2, presenting clearly that the organic components went

through notable volatilization under variable temperature conditions. If exposed in the stack for a long period, the adhesion and corrosion resistance of FRP would be affected.

With the increasing temperature, the resin molecules transformed from glassy to high-elastic state, where the molecular chain stretched up and its elastic strain elongated to several times of its original length. However, when the temperature plunged, the contraction of the molecular chain was too slow to restore to its original state, which was the reason cracks occurred. Bubbles also existed on the surface of sample, and the coatings were found delaminating from the steel substrate clearly. Bubbles appear because the molecular chains of the phenolic resin were inclined to degradation under high temperature. Delamination was the reflection of the thermal expansion variation between organic coatings and steel substrates. In view of FRP, other than color changes, samples exhibited remarkable toughness on the material surface. Stevanovic et al. (2003) reported two main toughening mechanisms within the composites. First, the plastic deformation of the materials was considered to be the major toughening mechanism. Second, various forms of cracking were proven to influence the fracture toughness. As for VEGF, a relatively short time scale would not affect the coatings combined with the steel substrate, but a prolonged period of variable temperature environment may affect the material's coating properties. Moreover, the visibly yellow color and surface deformation denoted that FRP was less resistant to variable temperature conditions in power plant stacks. The utilization of FRP may lead to corrosion failure in the long run.

Negligible change took place in the sample weight as well as the appearance for titanium alloy and ND steel. The mass loss of foam glass blocks was merely 0.196 mg/cm^2, which indicated that it only underwent slight volatilization under variable temperature. It is revealed that these three materials could withstand dramatic temperature increase or decrease, and were suitable for the variable temperature conditions of power plant stacks following WFGD system.

Accelerated corrosion test

The first group was under static acid condensation conditions and the second group was under cyclic wet-dry conditions for all the experimental materials. Figure 2 denotes that weight loss occurred to both groups under different conditions for polyurea, VEGF and FRP. In view of polyurea, the corrosion rate of the first group was relatively smaller than the second group. The sample color became dark, and cracks occurred at the edges of the samples under alternating wet and dry conditions. The

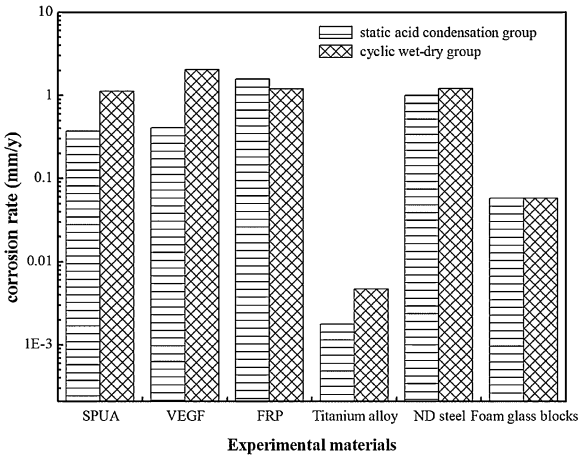

Fig. 2 Corrosion rates of six experimental materials after accelerated corrosion test under various conditions: for static acid condensation group, samples were immersed in 50 °C acid for 144 h; for cyclic wet-dry group, samples were immersed in 50 °C acid for 108 h and were placed in 120 °C for 18 h

soaking solution deepened significantly, transforming from transparent to red after acid immersion test, indicating that polyurea could dissolve into the acid solution. As for VEGF, the corrosion rate of the first group was low, the color changed slightly, and bubbles appeared on the sample surface. In sum, the corrosion rate of the second group increased dramatically. Other than bubbling, slight cracks appeared as well. Scratches were able to be distinguished, and the delamination of the coatings from the steel substrate could also be observed. The corrosion rate of the first FRP samples was relatively higher; indicating that longer period of acid immersion might place a more significant impact on FRP. The corrosion rate of the second group of samples was relatively low, however, the sample surface became yellow, dull and dark compared to the first group of FRP.

As for the organic coatings such as polyurea, VEGF and FRP, the molecules transformed from the glass state to the elastomeric state under high temperature conditions. The molecular chains stretched up, and the elastic strain increased to several times of its original length. When temperature decreased, the molecular chains shrank too slowly to restore to its original state, and cracking occurred. The acid condensation penetrated directly through the cracks and crevices, deteriorating the corrosion of the steel substrate dramatically for polyurea and VEGF. The dispersion of pores on VEGF surface may be due to the fact that phenolic groups of resin molecule were prone to decomposition during the immersion of the acid. The released gases resulted in the bubbly phenomenon. The deformation of FRP samples could be

explained by the similar mechanism mentioned in previous high temperature test. It could be demonstrated that polyurea was less resistant to static acid condensation environments as well as cyclic wet-dry conditions. Experiments revealed that the influence of corrosive environment created by static acid condensation was relatively milder. VEGF and FRP samples could not withstand the repeated cyclic wet-dry environments.

The corrosion rate of ND steel was relatively larger in the second group samples for ND steel, which indicated that the alternating change between high and low temperature, dry and moist environment would increase the corrosion rate of this material. Significant corrosion existed at the edges of both sets of samples, and corrosion products precipitated in the experimental liquid. Corrosion products appeared on the surface of both sets of samples, while the surface under different corrosion environments exhibited totally different. Red corrosion products presented in static acid condensation; in contrast, black corrosion products dominated the sample surface under cyclic wet-dry conditions. The dominant morphology was pitting for the first group whereas cracks associated with craters were the main morphology for the second group. Craters were distributed along the cracking line. It can be seen that the cracks and craters could nucleate and propagate in the upper regions whereas numerous vague ridge-like structures dispersed prominently on the nether part of the specimen surface for the second group. The steel substrate of the latter was corroded more deeply compared to the former group.

The corrosion rate of titanium alloy was nearly to zero for each sample of the first and the second group, with the average of 0.00319 and 0.00845 mm/y, respectively. This may be attributed to the compact oxide film generated on the surface of titanium alloy that prevented further corrosion. Besides, no significant color change or obvious corrosion took place on the surface, indicating that its corrosion resistance to acid and to cyclic conditions was excellent compared to conventional materials. It could be concluded that titanium alloy can be used as stack lining materials.

Titanium demonstrated an outstanding corrosion resistance owing to the formation of stable and dense titanium oxides, mainly TiO_2, on the surface of the metal (Mabilleau et al. 2006; Bloyce et al. 1998). The excellent corrosion resistance of titanium resulted from the formation of this continuous, highly adherent and protective oxide films. Titanium had high corrosion resistance to many media, but its corrosion resistance was poor in sulfuric acid at high temperature. However, alloying with nickel and molybdenum could substantially improve the corrosion resistance. Molybdenum provided protection against corrosion attack through stable passivation in aggressive environments, while nickel promoted the formation of nickel titanium and the passivity of titanium in the acid environments (Sugizaki et al. 1996; Bloyce et al. 1998). The complementary effects of molybdenum with nickel were to enhance the corrosion behavior of titanium in sulfuric acid solution (Sugizaki et al. 1996; Blanco-Pinzon et al. 2005). These elements were also effective in improving the resistance to crevice attack in chloride media, which was the main ion content in acid condensation of power plant stacks. And the protection against such corrosion attack was reported to be maintained for long-term exposure to the corrosive environment. Besides, literatures had been reported lately that palladium (Pd) implanted could promote the passivation of titanium and produce an outstanding resistance to strong acids (Blanco-Pinzon et al. 2005; Brossia and Cragnolino 2004). This element could strengthen the passive film of titanium, and made the alloy immune to acid condensation. Furthermore, tantalum (Ta) was an element that could preferentially suppress the dissolution of titanium. This conclusion was in agreement with that of bulk alloying with tantalum, which showed improvement of corrosion resistance in hydrochloric acid solution for titanium steel (Sugizaki et al. 1996). Being combined with molybdenum, nickel, palladium, or tantalum, the corrosion resistance of titanium had been remarkably improved.

It also could be seen that foam glass blocks in both the first and second group experienced no significant change in weight as well as appearance. This indicated the immersion in acid condensation or the exposure to cyclic wet-dry conditions had no significant effect on foam glass blocks. The minimal corrosion rates were 0.0580 and 0.0583 mm/y, denoting that foam glass blocks were very stable and were not selective to the outer environments. The excellent corrosion resistance could be explained by the protective silicon dioxide (SiO_2) and boron trioxide (B_2O_3) layer formed above the surface during the experimental process (Soo Park et al. 1999). Obviously, simultaneous accumulation of SiO_2 and B_2O_3 led to comparatively less loss of foam glass blocks on the glass surface.

Owing to its ability of surface restoration at elevated temperatures, foam glass blocks had the potential for use in corrosive environments in power plant. The higher corrosion loss was because of its porous structure, allowing easy acid penetration that led to the formation of cracks or open paths for corrosive attack. Instead, the slow corrosion rate of foam glass blocks was probably because of the formation of an oxidation layer of SiO_2 and B_2O_3 on the material surface. A uniform layer could appreciably decrease the surface porosity and thereby improve the corrosion resistance. The deceased pores on

the surface retarded the acid to penetrate and thus suppress the corrosive attack. The formed oxide layer had low porosity, making them less susceptible to corrosive degradation (Park et al. 2009; Keding et al. 2002; Littner et al. 2006). In other words, through pore-filling and planarization, the layer could improve the densification of the surface, and consequently, the corrosion resistance. The surface layer acted as a barrier to the corrosive environment for the foam glass blocks, which enhanced the corrosion resistance of the material in power plant stacks.

As illustrated in Fig. 2, it can be concluded that FRP and ND steel are the two materials that went through most dramatic weight loss after immersed in the acid condensation. Polyurea and VEGF also underwent minor weight loss, while there was almost no change for titanium alloy and foam glass blocks under the same experimental conditions. These results are in consistent with those under the cyclic wet-dry environments. As for VEGF, the corrosion rate was as high as around 2.02 mm/y; whereas for ND steel, FRP and polyurea, it was respectively 1.21, 1.19 and 1.12 mm/y, indicating the cyclic wet-dry environments placed a great damage to these four materials. Least loss occurred to titanium alloy and foam glass blocks. Titanium alloy was always stable in both corrosion environments mainly because of the formed adherent and protective surface oxidation films when implanted with different elements. Foam glass blocks embraced excellent corrosion resistance due to the formation and protection of SiO_2 and B_2O_3 layers.

Moreover, it can be concluded that cyclic wet-dry conditions would result in great damage to materials compared to the static acid condensation environments. This could be explained as follows: take ND samples as an example. When the specimen was first put in the acid condensation for a period, corrosion products were started to form on the surface, leading to the increase of corrosion rate of the sample. As time went by, pits and cracks gradually covered and distributed through the entire surface. When the sample was laid under high temperature, the hot environments would make the pitting, cracking and peeling even worse. Then the sample was replaced in the acid condensation again, where the corrosion was accelerated because the acid could easily go through the cracks and corrode the substrate underneath. The cyclic wet-dry environments could dramatically deteriorate the sample surface and increase the corrosion rate of the materials. In the real world, there are three working conditions in the power plant stacks, and the temperature as well as the acidity is always changing. In this way, the designed cyclic wet-dry conditions are more close to the real operating conditions of power plant stacks. That is to say, the materials to be utilized in stacks should be optimized to withstand this kind of environments.

Through the weight loss analysis, with the combination of surface characterization of each material, it can be concluded that the titanium alloy and foam glass blocks

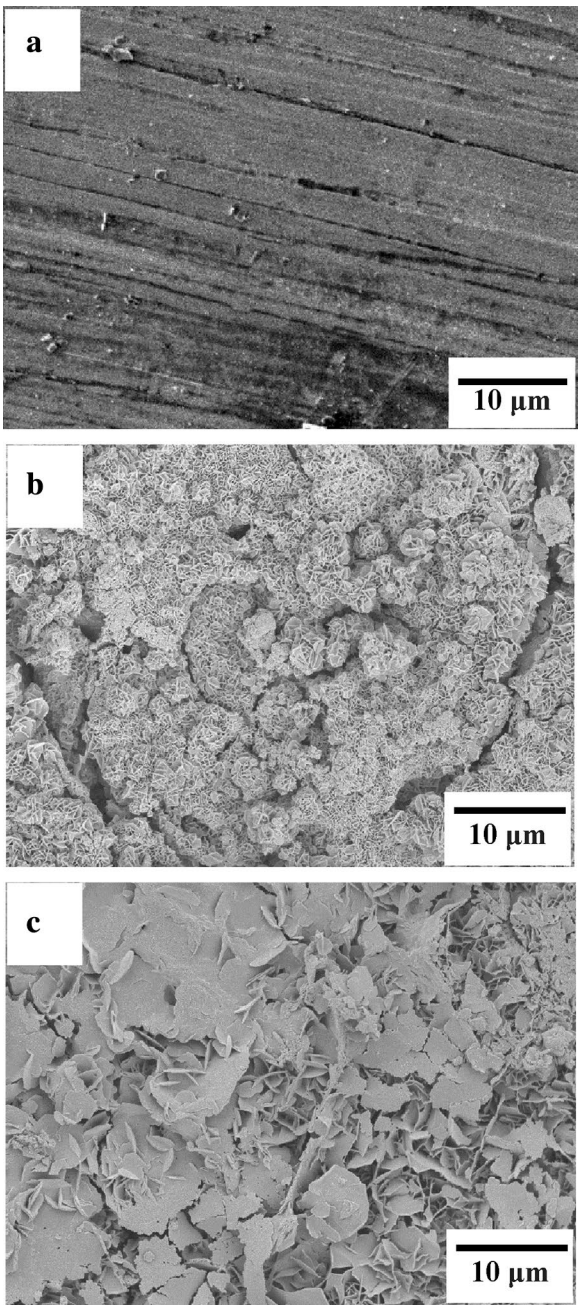

Fig. 3 SEM morphologies of ND steel after accelerated corrosion test under various conditions: **a** original samples; **b** static acid condensation group, samples were immersed in 50 °C acid for 144 h; **c** cyclic wet-dry group, samples were immersed in 50 °C acid for 108 h and were placed in 120 °C for 18 h

were two materials that were resistant to corrosion in comparison with the conventional materials.

SEM analysis

SEM analysis of ND steel

As illustrated in Fig. 3, numerous large pieces of pearlite extruded significantly from the sample surface for the first group. The uniform corrosion products were distributed as dots or clusters, with corrosion pits throughout the entire surface. The dominant surface morphology was pits for the first sample group while pitting associated with severe cracking was the major morphology for the second group. Corrosion products of the second group were composed of double layers-the bottom layer consisted of very fine grains bonded to the metal substrate, whereas on the upper layer, loose metal flakes presented. The inner corrosion layers were denser and more consolidated in needle-like or rectangular forms. The outer layers consisted of a higher degree of flake formation after cyclic wet-dry corrosion. The bottom substrate was corroded deeply, and the corrosion products demonstrated a cluster-like distribution, which fell off easily. There were large gouges and cracks among the corrosion products; at a few locations, the cracks were pronounced and extended into the substrate area. The cracks or holes could make the sample surface vulnerable to resist corrosion, and the acid could enter the steel matrix and accelerate corrosion. This was a significant difference compared to the morphology for the first group at the corresponding static acid conditions, where no flakes, no needle-like products, or less gouges were found. Comparison shows that ND steel is less corrosion resistant to cyclic wet-dry environments. It needs further treatment if utilized as the steel tube materials.

SEM analysis of foam glass blocks

No significant change occurred on the sample surface after the experiment, as shown in Fig. 4. No corrosion products could be observed. There were no signs of delamination, and no trace of spalling or cracking. The corrosion resistance of foam glass blocks is better than conventional materials.

XRD analysis

In order to reveal the corrosion mechanism of ND steel in both static acid condensation and cyclic wet-dry condition, the corrosion products were analyzed by an XRD. As illustrated in Fig. 5, it could be demonstrated that the dominant corrosion products were Fe_2O_3, $FeSO_4$, and FeOOH for the above two experimental conditions. However, Fe_3O_4 only exhibited in the static acid condensation group while FeF_3 was the specific product under the cyclic wet-dry conditions.

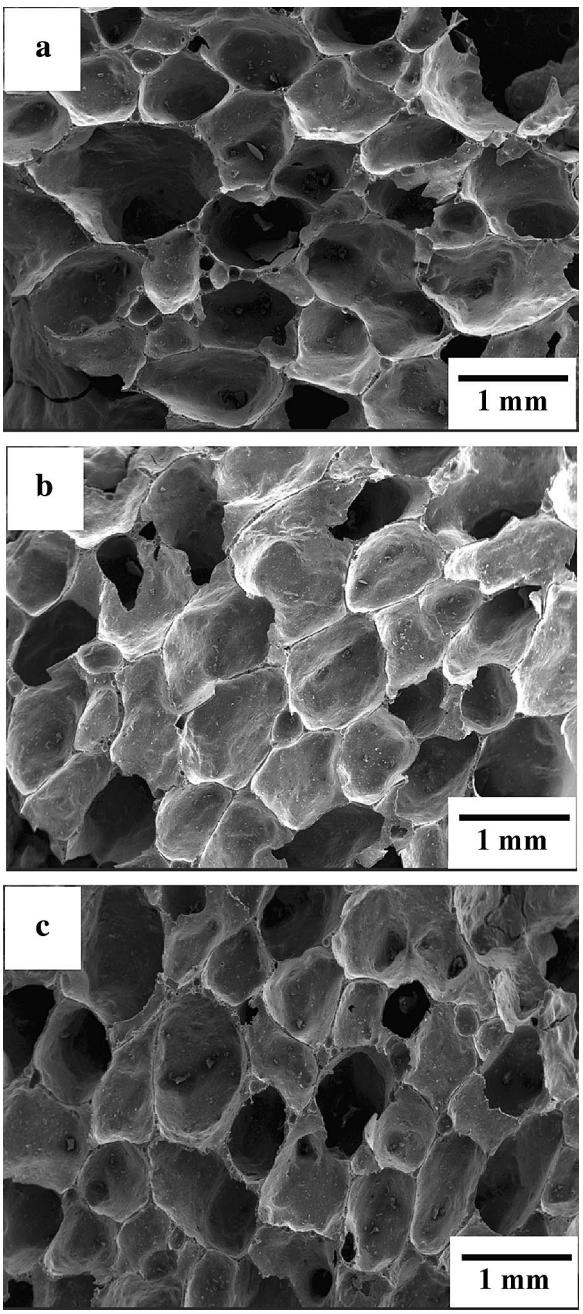

Fig. 4 SEM morphologies of foam glass blocks after accelerated corrosion test under various conditions: **a** original samples; **b** static acid condensation group, samples were immersed in 50 °C acid for 144 h; **c** cyclic wet-dry group, samples were immersed in 50 °C acid for 108 h and were placed in 120 °C for 18 h

The hydrolysis of iron led to the formation of ferric hydroxide under acidic conditions. Legrand and Leroy (1990) noted that ferric hydroxide was deposited on the inner wall of steel and iron pipe, this amorphous hydroxide was likely overtime, to lose water molecules (dehydrate),

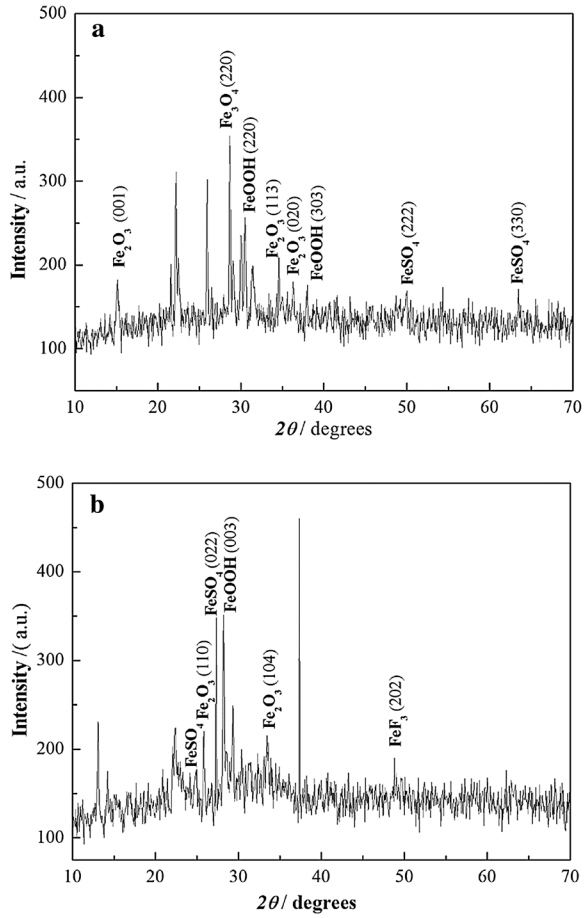

Fig. 5 Iron compounds in corrosion products of ND steel after accelerated corrosion test analysed by XRD: **a** static acid condensation group, samples were immersed in 50 °C acid for 144 h; **b** cyclic wet-dry group, samples were immersed in 50 °C acid for 108 h and were placed in 120 °C for 18 h

and to change slowly into other trivalent iron oxides such as FeOOH or Fe_2O_3. The ferrous ion reacted with the sulfate ion to form $FeSO_4$, which served as an incentive for corrosion. The accumulation of sulfate ions with the increase of the reaction time would lead to the continuous acceleration of corrosion reaction (Nishimura et al. 2004). Fe_3O_4 generally occurred under conditions of poor oxygen supply, and it could be the reason why Fe_3O_4 only formed in the static acid condition, where samples were immersed below the water lever during the entire experimental process. The formation of FeF_3 in the second group may result from the activity of F^- under cyclic wet-dry especially under elevated temperature conditions. It was denoted that a lower level of F^- caused an increasing effect on corrosion rate of steels with the rise in temperature (Singh et al. 2002).

Conclusions

- The performance analysis and comparative studies of six materials for the prevention of stack corrosion were investigated under WFGD conditions in coal-fired power plants. Titanium alloy and foam glass blocks had the best performance and could be applied in the stack to prevent corrosion.
- Ion chromatography revealed that the acid condensation mainly contains F^-, Cl^-, NO_3^-, SO_4^{2-} and SO_3^{2-}, making the inner wall of stack a highly corrosive environment.
- The corrosion of VEGF and FRP would lead to degradation or failure because of the cracks or deformation. Alloying with nickel and molybdenum could substantially improve the corrosion resistance of titanium alloy. The formation of SiO_2 and B_2O_3 layers contributed to the stability of foam glass blocks. The dominant morphologies of ND steel were dots and pits in acid condensation; while cracks with flakes were the major products under cyclic wet-dry conditions. Corrosion products were predominantly composed of Fe_2O_3, $FeSO_4$, and FeOOH, with Fe_3O_4 or FeF_3.
- The cyclic wet-dry environments impaired the corrosion resistance of materials and caused more corrosion damage compared to acid condensation. The effects of cyclic wet-dry conditions should be taken into account to mitigate the corrosion in stacks of coal-fired power plant.

Authors' contributions

ZS did all the experimental design and most of the experiments. ZY did the literature review regarding all the anticorrosion methods of stack in power plants. HY conducted the XRD analysis. AC helped to analyze the results from SEM analysis. WJ helped with the measurement of all the ions in acid condensation. YY helped with the temperature tests. All authors read and approved the final manuscript.

Author details

[1] Institute for Energy, Environment and Sustainability Research, UR-NCEPU, University of Regina, Regina, SK S4S 0A2, Canada. [2] School of Environmental Science and Engineering, North China Electric Power University, Baoding 071003, People's Republic of China. [3] School of Mathematics and Physics, North China Electric Power University, Baoding 071003, China. [4] Key Laboratory of Beijing for Water Quality Science and Water Environment Recovery Engineering, Beijing University of Technology, Beijing 100124, China.

Acknowledgements

We are also grateful for the support from the Faculty of Environmental Science and Engineering, North China Electric Power University.

Competing interests

The authors declare that they have no competing interests.

Received: 18 July 2016 Accepted: 18 August 2016
Published online: 31 August 2016

References

Blanco-Pinzon A, Liu Z, Voisey K, Bonilla FA, Skeldon P, Thompson GE, Piekoszewski J, Chmielewski AG (2005) Excimer laser surface alloying of titanium with nickel and palladium for increased corrosion resistance. Corros Sci 47:1251–1269

Bloyce A, Qi PY, Dong H, Bell T (1998) Surface modification of titanium alloys for combined improvements in corrosion and wear resistance. Surf Coat Technol 107:125–132

Brossia CS, Cragnolino GA (2004) Effect of palladium on the corrosion behavior of titanium. Corros Sci 46:1693–1711

Cai JM, Huang X, Cao CX, Ma JM (2010) Thermal stability of TG6 titanium alloy and its partial resumption at high temperature. Rare Metal Mat Eng 39:1893–1898

Ghanem WA, Bayyoumi FM, Ateya BG (1996) The high temperature corrosion of a low alloy steel in aqueous sodium chloride. Corros Sci 38:1171–1186

González-Guzmán J, Santana JJ, González S, Souto RM (2010) Resistance of metallic substrates protected by an organic coating containing glass flakes. Prog Org Coat 68:240–243

Grujicic M, Pandurangan B, He T, Cheeseman BA, Yen CF, Randow CL (2010) Computational investigation of impact energy absorption capability of polyurea coatings via deformation-induced glass transition. Mater Sci Eng A 527:7741–7751

Gutiérrez Ortiz FJ, Ollero P (2008) Modeling of the in-duct sorbent injection process for flue gas desulfurization. Sep Purif Technol 62:571–581

Hu W, Tanaka K, Haddad PR, Hasebe K (2000) Suppressed electrostatic ion chromatography with tetraborate as eluent and its application to the determination of inorganic anions in snow and rainwater. J Chromatogr A 884:161–165

Jang HJ, Kim RH, Kwon HS, Kim TS, Cho KC, Choi JS, Heo TY, Lee JH (2009) Study on corrosion resistance of gas cylinder materials in HF, HCl and HBr environments. Corros Eng Sci Technol 44:445–452

Jeon SH, Kim ST, Lee IS, Park JH, Kim KT, Kim JS, Park YS (2011) Effects of copper addition on the formation of inclusions and the resistance to pitting corrosion of high performance duplex stainless steels. Corros Sci 53:1408–1416

Keding R, Rüssel C, Pascual MJ, Pascual L, Durán A (2002) Corrosion mechanism of borosilicate sealing glasses in molten carbonates studied by impedance spectroscopy. J Electroanal Chem 528:184–189

Legrand L, Leroy P (1990) Prevention of corrosion and scaling water supply systems. Ellis Horwood, New York

Littner A, Allemand BG, François M, Vilasi M (2006) Molten glass corrosion resistance of MoxRuySiz compounds at 1350 & #xB0;C in an alkali borosilicate glass. Corros Sci 48:1426–1436

Lu Z, Liu Y, Barreto V, Pohl C, Avdalovic N, Joyce R, Newton B (2002) Determination of anions at trace levels in power plant water samples by ion chromatography with electrolytic eluent generation and suppression. J Chromatogr A 956:129–138

Mabilleau G, Bourdon S, Joly-Guillou ML, Filmon R, Baslé MF, Chappard D (2006) Influence of fluoride, hydrogen peroxide and lactic acid on the corrosion resistance of commercially pure titanium. Acta Biomater 2:121–129

Moser P, Schmidt S, Uerlings R, Sieder G, Titz JT, Hahn A, Stoffregen T (2011) Material testing for future commercial post-combustion capture plants-Results of the testing programme conducted at the Niederaussem pilot plant. Energy Procedia 4:1317–1322

Nam ND, Kim MJ, Jang YW, Kim JG (2010) Effect of tin on the corrosion behavior of low-alloy steel in an acid chloride solution. Corros Sci 52:14–20

Ni H, Johnson AH, Soucek MD, Grant JT, Vreugdenhil AJ (2002) Polyurethane/polysiloxane ceramer coatings: evaluation of corrosion protection. Macromol Mater Eng 287:470–479

Nishimura R, Shiraishi D, Maeda Y (2004) Hydrogen permeation and corrosion behavior of high strength steel MCM 430 in cyclic wet–dry SO_2 environment. Corros Sci 46:225–243

Noubactep C (2010) The suitability of metallic iron for environmental remediation. Environ Prog Sustain Energy 29:286–291

Park JS, Taniguchi S, Park YJ (2009) Alkali borosilicate glass by fly ash from a coal-fired power plant. Chemosphere 74:320–324

Qiao J, Amirkhizi AV, Schaaf K, Nemat-Nasser S, Wu G (2011) Dynamic mechanical and ultrasonic properties of polyurea. Mech Mater 43:598–607

Roberts DRT, Holder SJ (2011) Mechanochromic systems for the detection of stress, strain and deformation in polymeric materials. J Mater Chem 21:8256–8268

Russel WB (2011) Mechanics of drying colloidal dispersions: fluid/solid transitions, skinning, crystallization, cracking, and peeling. AIChE J 57:1378–1385

Santoyo E, Verma SP, Sandoval F, Aparicio A, García R (2002) Suppressed ion chromatography for monitoring chemical impurities in steam for geothermal power plants. J Chromatogr A 949:281–289

Sedyohutomo A, Lim LW, Takeuchi T (2008) Development of packed-column suppressor system for capillary ion chromatography and its application to environmental waters. J Chromatogr A 1203:239–242

Siamphukdee K, Collins F, Zou R (2013) Sensitivity analysis of corrosion rate prediction models utilized for reinforced concrete affected by chloride. J Mater Eng Perform 26:1531–1540

Singh DDN, Ghosh R, Singh BK (2002) Fluoride induced corrosion of steel rebars in contact with alkaline solutions, cement slurry and concrete mortars. Corros Sci 44:1713–1735

Song S, Wen Z, Liu Y, Wu X, Lin J (2011) Bi-doped borosilicate glass as sealant for sodium sulfur battery. J Non-Cryst Solids 357:3074–3079

Soo Park Y, Butt DP, Castro R, Petrovic J, Johnson W (1999) Durability of molybdenum disilicide in molten alkali borosilicate glass. Mater Sci Eng A 261:278–283

Stevanovic D, Kalyanasundaram S, Lowe A, Jar PYB (2003) Mode I and mode II delamination properties of glass/vinyl-ester composite toughened by particulate modified interlayers. Compos Sci Technol 63:1949–1964

Sugizaki Y, Yasunaga T, Tomari H (1996) Improvement of corrosion resistance of titanium by co-implantation. Surf Coat Technol 83:167–174

ZareNezhad B, Aminian A (2010) A multi-layer feed forward neural network model for accurate prediction of flue gas sulfuric acid dew points in process industries. Appl Therm Eng 30:692–696

Zhao Y, Han YH, Ma T, Guo TX (2011a) Simultaneous desulfurization and denitrification from flue gas by Ferrate (VI). Environ Sci Technol 45:4060–4065

Zhao Y, Guo TX, Chen Z (2011b) Experimental study on simultaneous desulfurization and denitrification from flue gas with composite absorbent. Environ Prog Sustain Energy 30:216–220

Zivojinovic DZ, Rajakovic LV (2011) Application and validation of ion chromatography for the analysis of power plants water: analysis of corrosive anions in conditioned water-steam cycles. Desalination 275:17–25